

Article

# Impact of Improved Mellor–Yamada Turbulence Model on Tropical Cyclone-Induced Vertical Mixing in the Oceanic Boundary Layer

Taekyun Kim  and Jae-Hong Moon \*

Department of Earth and Marine Science, College of Ocean Sciences, Jeju National University, Jeju 63243, Korea; tkkim79@gmail.com

\* Correspondence: jhmoon@jejunu.ac.kr

Received: 15 June 2020; Accepted: 5 July 2020; Published: 6 July 2020



**Abstract:** It has been identified that there are several limitations in the Mellor–Yamada (MY) turbulence model applied to the atmospheric mixed layer, and Nakanishi and Niino proposed an improved MY model using a database for large-eddy simulations. The improved MY model (Mellor–Yamada–Nakanishi–Niino model; MYNN model) is popular in atmospheric applications; however, it is rarely used in oceanic applications. In this study, the MY model and the MYNN model are compared to identify the efficiency of the MYNN model incorporated into an ocean general circulation model. To investigate the impact of the improved MY model on the vertical mixing in the oceanic boundary layer, the response of the East/Japan Sea to Typhoon Maemi in 2003 was simulated. After the typhoon event, the sea surface temperature obtained from the MYNN model showed better agreement with the satellite measurements than those obtained from the MY model. The MY model produced an extremely shallow mixed layer, and consequently, the surface temperatures were excessively warm. Furthermore, the near-inertial component of the velocity simulated using the MY model was larger than that simulated using the MYNN model at the surface layer. However, in the MYNN model, the near-inertial waves became larger than those simulated by the MY model at all depths except the surface layer. Comparatively, the MYNN model showed enhanced vertical propagation of the near-inertial activity from the mixed layer into the deep ocean, which results in a temperature decrease at the sea surface and a deepening of the mixed layer.

**Keywords:** turbulent mixing; improved Mellor–Yamada turbulence model; ocean boundary layer; typhoon

## 1. Introduction

Turbulence in the oceanic boundary layer (OBL) is of paramount importance because it vertically transports heat and momentum. Consequently, oceanic vertical mixing due to turbulence plays an essential role in ocean dynamics. In particular, it creates a homogeneous ocean layer (i.e., mixed layer) that interacts directly with the atmosphere. As a key parameter controlling atmosphere–ocean interactions across the air–sea interface, vertical mixing in upper ocean plays a critical role in regulating the sea surface temperature (SST). The air–sea interaction through the SST significantly influences many atmospheric and oceanic phenomena by determining the momentum and enthalpy exchange between the atmosphere and the ocean [1–4]. In particular, it plays a vital role in the occurrence and development of severe weather events originating from the ocean, such as tropical cyclones (TCs) [5]. SST has long been considered one of the governing factors in tropical storm intensity; high SSTs are well known to provide favorable conditions that intensify TCs and vice versa [6,7]. Furthermore, it is widely known that TC-induced strong surface winds cause intense turbulent mixing in the upper ocean

layer. The resonant inertial oscillation responses of the upper ocean to TC-related strong surface winds make vertical shear at the base of the OBL intense, and consequently to amplified inertial motions that drive turbulent mixing in the thermocline and interior ocean [8]. The near-inertial energy can be transferred to the deep ocean [9–12]. Vincent et al. [13] discussed the ocean response to TC transits by investigating the integrated impact of TCs on the seasonal ocean thermal structure and heat transport. They found that the climatological ocean state is closely influenced by TC wind-driven surface heat fluxes, TC-induced oceanic vertical mixing, and advective processes.

Therefore, oceanic vertical mixing must be correctly estimated. However, vertical mixing usually cannot be explicitly represented in the ocean general circulation model (OGCM) because of the small-scale turbulent processes involved. Therefore, it has to be parameterized; that is, the effects of the turbulent phenomena are to be expressed using synoptic state variables. A number of high-order turbulence closure models have been developed since the 1970s. Among these models, the Mellor–Yamada (MY) model [14–17] has been commonly used to model experiments and operational numerical predictions. One of the reasons for preferring the MY model is that although a minimum number of closure constants is used in the MY model, it acceptably reproduces the measured non-dimensional universal functions in the surface layer [18]. Furthermore, the MY model has a relatively low computational cost; consequently, it is popular in both operational weather forecasts and research models [19,20]. The MY model has been widely used in geophysical applications such as modeling the atmospheric and oceanic boundary layers [21,22]. However, several deficiencies have been highlighted regarding the MY model. These include certain limitations in the MY model that have been identified by many researchers regarding the atmospheric mixed layer, slowly growing a convective boundary layer [23], and rapidly decaying turbulence in a stable nocturnal boundary layer [24].

Several authors have attempted to address the problems in the MY model, suggesting a variety of alternatives for the coefficient values and functional representations [25–29]. Among them, Nakanishi and Niino [30] recently proposed an improved MY model using a database for large-eddy simulations (LESs). The improvements to the model include (1) a newly designed formula for the turbulent length scale (TLS) realistically increasing with a decrease in stability, (2) parameterization of the pressure covariances, and (3) expression of stability functions for 3rd-order turbulent fluxes [30,31]. Consequently, the model improved several limitations in the MY model, for example, the insufficient growth of the convective boundary layer, and underestimated turbulent kinetic energy (TKE) and the TLS. This improved MY model by Nakanishi and Niino (Mellor–Yamada–Nakanishi–Niino model; MYNN model) has been observed to provide good performance [30] and has been incorporated into atmospheric general circulation models, such as an operational weather prediction model at the Japan Meteorological Agency [32,33], MIROC (Model for Interdisciplinary Research On Climate) at the Frontier Research Center for Global Change [34], and WRF (Weather Research and Forecasting).

The MYNN model has proven to be popular in atmospheric applications. On the other hand, it has rarely been used in oceanic applications, except in a number of numerical experiments. Using a LES, Furuichi et al. [35] and Furuichi and Hibiya [36] assessed the turbulence closure models in the OBL using a LES and compared this with the results of the boundary layer models. In addition, a study using the MYNN model for typhoon-induced ocean response was conducted by Suzuki et al. [37] and Shibano et al. [38]. However, an idealized experiment was used in their studies. Furthermore, Kanada et al. [39] carried out realistic simulations for the response of the oceans to typhoons and the feedback to typhoons using an atmosphere–ocean coupling model that consists of an ocean model with the MYNN model, but they focus on the typhoon responses to the SST simulated in the coupled model system.

In this study, to compare and assess oceanic responses for two mixed-layer parameterizations, we applied the improved MY model to an oceanic scenario and investigated the influence of the MYNN model for the oceanic mixed layer on TC-induced vertical mixing. Accordingly, each of the level 2.5 version of the MY and the level 2.5 version of the MYNN were incorporated into an ocean general

circulation model, and subsequently, the ocean response to the TC-induced vertical mixing simulated by each parameterization was systematically compared.

## 2. Vertical Mixing Processes

The vertical turbulent fluxes in the equation for the large-scale physical quantity can be parameterized as follows:

$$-\langle uw \rangle = K_M \frac{\partial U}{\partial z}, \tag{1}$$

$$-\langle vw \rangle = K_M \frac{\partial V}{\partial z}, \tag{2}$$

$$-\langle w\theta \rangle = K_H \frac{\partial \Theta}{\partial z}, \tag{3}$$

where  $U$  and  $V$  are the zonal and meridional mean velocities,  $\Theta$  is the mean potential temperature, and  $u$ ,  $v$ ,  $w$ , and  $\theta$  are the fluctuation components of the velocity and temperature, respectively. The mathematical relationship shows the aforementioned assumption that the turbulent fluxes are proportional to the gradient of the large-scale values. Ultimately, solving the mixed layer model provides the momentum and heat-flux coefficients,  $K_M$  and  $K_H$ , respectively.

In the turbulence closure models, the vertical eddy viscosity  $K_M$  and diffusivity  $K_H$  are estimated as follows:

$$K_M = lqS_M, \tag{4}$$

$$K_H = lqS_H, \tag{5}$$

where  $q$  is the turbulent velocity,  $l$  is the TLS, and  $S_M$  and  $S_H$  are the stability functions.

The stability functions are derived algebraically using the simultaneous equation for  $S_M$  and  $S_H$ .

$$S_M = f\left(l, q, \frac{\partial U}{\partial z}, \frac{\partial V}{\partial z}, N^2\right), \tag{6}$$

$$S_H = f\left(l, q, \frac{\partial U}{\partial z}, \frac{\partial V}{\partial z}, N^2\right), \tag{7}$$

where  $N$  is the buoyancy frequency.

Using  $S_M$  and  $S_H$ ,  $K_M$  and  $K_H$  are obtained by determining  $q$  and  $l$ . The level 2.5 model is composed of the time-evolving equation for the TKE and the algebraic equation for the other second-moment turbulent quantities. The time-evolution equation for the TKE is given by the following equation:

$$\frac{D}{Dt} \left( \frac{q^2}{2} \right) - \frac{\partial}{\partial z} \left[ qlS_q \frac{\partial}{\partial z} \left( \frac{q^2}{2} \right) \right] = P_s + P_b - \varepsilon, \tag{8}$$

where  $P_s (= qlS_M \left\{ \left( \frac{\partial U}{\partial z} \right)^2 + \left( \frac{\partial V}{\partial z} \right)^2 \right\})$  and  $P_b (= qlS_H N^2)$  are the shear and buoyancy production of the TKE, respectively.  $S_q$  is another stability function and energy dissipation term where the length scale ( $\Lambda_1 = B_1 l$ , where  $B_1$  is the closure constant) is given as follows:

$$\varepsilon = \frac{q^3}{\Lambda_1}. \tag{9}$$

Here, we briefly introduce some distinctions of the MYNN model because the MY model has already been described in the published literature (e.g., [15,16,40,41]). There are three main deficiencies in the second-order closure models, which have been identified in the previous study [42]; (1) neglected buoyancy effects for the pressure covariances, (2) uncertainty expressed for a length scale, and (3) down-gradient-diffusion assumption for the turbulent transport.

Nakanishi and Niino [30] attempted to improve two MY model deficiencies based on data constructed using LES. For the first MY model deficiency, they added parameterization of the buoyancy effects for the pressure covariances to the MY model as follows:

$$\begin{aligned} \left\langle \frac{p}{\rho_0} \left( \frac{\partial u_i}{\partial x_j} + \frac{\partial u_j}{\partial x_i} \right) \right\rangle &= -\frac{q}{3A_1 l} \left( \langle u_i u_j \rangle - \frac{1}{3} q^2 \delta_{ij} \right) + C_1 q^2 \left( \frac{\partial U_i}{\partial x_j} + \frac{\partial U_j}{\partial x_i} \right) \\ &+ C_2 \frac{g}{\rho_0} \left( \langle u_i \rho \rangle \delta_{j3} + \langle u_j \rho \rangle \delta_{i3} - \frac{1}{3} \langle u_k \rho \rangle \delta_{ij} \right) \\ &+ C_4 \left( \langle u_i u_k \rangle \frac{\partial U_j}{\partial x_k} + \langle u_i u_k \rangle \frac{\partial U_i}{\partial x_k} - \frac{2}{3} \langle u_i u_k \rangle \frac{\partial U_k}{\partial x_i} \delta_{ij} \right) \end{aligned} \tag{10}$$

$$\left\langle \frac{p}{\rho_0} \frac{\partial \theta}{\partial x_i} \right\rangle = -\frac{q}{3A_2 l} \langle u_i \theta \rangle - C_3 \frac{g}{\rho_0} \langle \theta \rho \rangle \delta_{i3} + C_5 \langle u_k \theta \rangle \frac{\partial U_i}{\partial x_k}, \tag{11}$$

where  $\delta_{ij}$  is Kronecker’s delta, which is unity for  $i = j$  and zero for  $i \neq j$ .  $A_1, A_2$ , and  $C_1 - C_5$  are closure constants. The terms with  $C_1, C_4$ , and  $C_5$  represent the effect of shear, and those with  $C_2$  and  $C_3$  represent the effect of buoyance.

The essence of the MY model is simple empirical constants that are determined from the experimental data for neutral stratification. However, this simplistic parameterization for the closure formation of the pressure–velocity and pressure–temperature correlations in the second moments equations is a limitation of the MY model where certain oversimplifications of the parameters can lead to less accurate results. Namely, the above terms with  $C_2 - C_5$  are neglected in the MY model: Mellor and Yamada [15] employ the empirical constants as

$$\begin{aligned} (A_1, A_2, B_1, B_2, C_1) &= (0.92, 0.74, 16.6, 10.1, 0.08), \\ (C_2, C_3, C_4, C_5) &= (0, 0, 0, 0), \end{aligned} \tag{12}$$

Nakanishi and Niino [30] revise the parameterization of the pressure covariances from the MY model. Moreover, they suggest an effective estimation for the level 3 model and the closure constants based on the LES results as follows:

$$\begin{aligned} (A_1, A_2, B_1, B_2, C_1) &= (1.18, 0.665, 24.0, 15.0, 0.137), \\ (C_2, C_3, C_4, C_5) &= (0.75, 0.352, 0, 0.2). \end{aligned} \tag{13}$$

For the second MY model deficiency, that is, the uncertainty expression for the master length scale  $l$ , they introduced a new diagnostic equation for  $l$  on the basis of the LES as follows:

$$l = \left( \frac{1}{L_s} + \frac{1}{L_T} + \frac{1}{L_B} \right)^{-1}, \tag{14}$$

where

$$L_s = \begin{cases} kz/3.7 & , \zeta \geq 1 \\ kz(1 + 2.7\zeta)^{-1} & , 0 \leq \zeta \leq 1 \\ kz(1 - 100\zeta)^{0.2} & , \zeta < 0 \end{cases} \tag{15}$$

is the length scale in the surface layer with  $\zeta (= z/L_M)$  being the dimensionless height  $L_M$ , the Monin–Obukhov length.

$$L_T = 0.23 \frac{\int_{-D}^0 qz dz}{\int_{-D}^0 q dz} \tag{16}$$

is the length scale dependent on the depth of the boundary layer.

$$L_B = \begin{cases} q/N & , N^2 > 0 \ \& \ \zeta \geq 0 \\ [1 + 5(q_c/L_T N)^{0.5}]q/N & , N^2 > 0 \ \& \ \zeta < 0 \\ \infty & , N^2 < 0 \end{cases} \quad (17)$$

is related to the buoyancy length scale with  $q_c (= (BL_T)^{1/3})$  being a velocity scale, and  $B$  being the buoyancy flux ( $m^2/s^{-3}$ ).

The new equation allows in the surface layer to vary with stability and provides values for the upper part of the convective boundary layer with little underestimation.

### 3. Methodology

For the numerical simulation, we used the Research Institute for Applied Mechanics (RIAM) Ocean Model (RIAMOM; Lee [43]) developed at the Kyushu University, Japan. RIAMOM is a three-dimensional, z-coordinate, and primitive equation OGCM that assumes hydrostatic balance with the Boussinesq approximation. The model covers the entire East/Japan Sea (EJS) from longitude 126.5° E to 142.5° E and latitude 33° N to 52° N with 1/12° in horizontal resolution and 36 vertical levels (Figure 1). The bottom topography was extracted from a combination of two topographic datasets, ETOPO5 and SKKU [44]. Further details and validation of the RIAMOM used in this study can be found in Kim and Yoon [45].

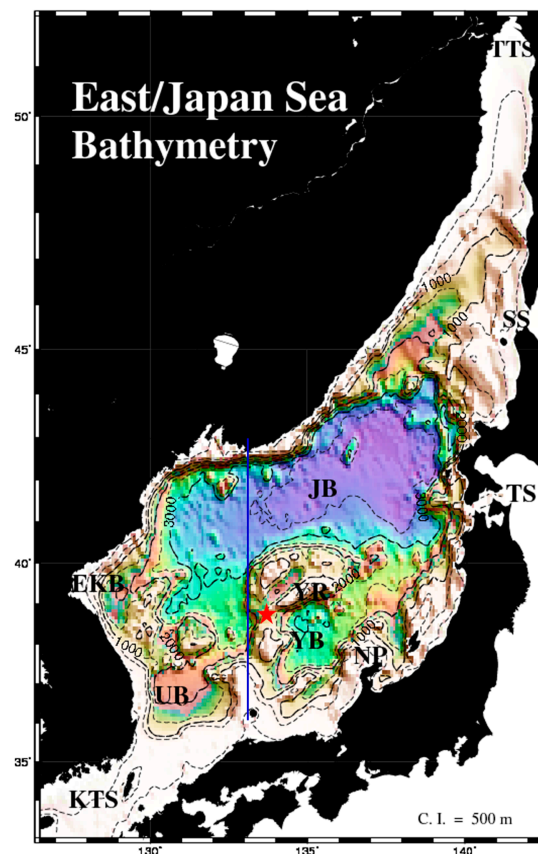


**Figure 1.** Study area and bathymetry (m). The contour interval is 500 m. KTS: Korea/Tsushima Strait, TS: Tsugaru Strait, SS: Soya Strait, TTS: Tatar Strait, UB: Ulleung Basin, YB: Yamato Basin, JB: Japan Basin, YR: Yamato Rise, EKB: East Korean Bay, NP: Noto Peninsula. The solid blue line along the 133° E line is for the vertical section and the red star denotes the position of the site used for the analysis related to the near-inertial motions.

The largest changes of the momentum budget in the OBL are caused by strong storms on a synoptic scale. TC-induced vertical mixing is responsible for significantly altering the thermal conditions in the ocean. The direction of the wind stress due to the storms can vary rapidly and force ocean currents that have a strong inertial oscillation. To investigate the impact of the improved MY model on TC-induced vertical mixing, the response of the boundary layer in the EJS to Super Typhoon Maemi in September 2003 was simulated. Typhoon Maemi was one of the strongest typhoons to ever hit the Korean Peninsula. The one-minute sustained wind speed reached approximately 280 km/h. It went through the center of the EJS, maintaining its strength (Figure 2). The reasons for maintaining much of its intensity were the warmer-than-usual SST of about 1.5–2 °C in the western Pacific Ocean and the fast moving speed.

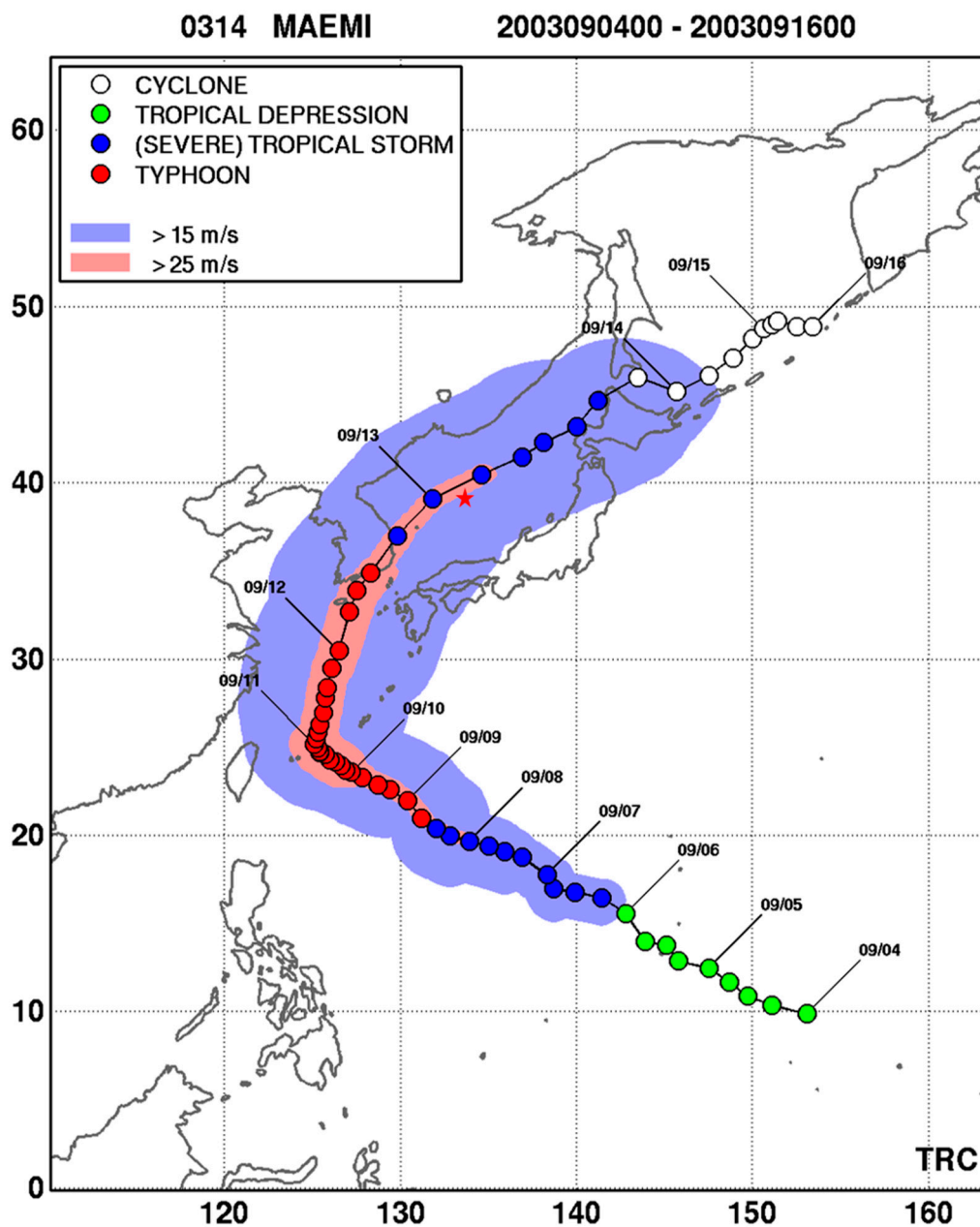


**Figure 2.** Best tracks of the Super Typhoon Maemi in September 2003 obtained from the Typhoon Research Center, Korea [46] (17 May 2020). The red star denotes the position of the site used for the analysis related to the near-inertial motions in Figures 7–9.

To examine the performance of the improved MY model for the OBL, we incorporated each vertical mixing parameterization into the RIAMOM and performed two numerical experiments on the sensitivity of the OBL to the vertical mixing parameterization using the MY and MYNN models, respectively. Numerical simulations were constructed to compare the response of the OBL to each turbulence model. Hourly wind stress data and the daily mean surface heat flux obtained from the Japan Meteorological Agency-Meso-Scale Model (JMA-MSM) with a resolution of 10 km [47] were used to compute the surface boundary conditions for the surface forcing. The open boundary conditions for the temperature and salinity in the inflow region were obtained from the operational version of RIAMOM [48]. The barotropic velocity through the Korea/Tsushima Strait was determined by the volume transport estimated from the long-term current observation data obtained from acoustic Doppler current profiler (ADCP) observations [49]. The daily mean results of the RIAMOM assimilation model [50] from the end of August 2003 were used for the initial conditions, and each run was integrated for 30 days from September 1 to 30.

## 4. Results

### 4.1. Response of the Upper Ocean Temperature

Figure 2 displays the pathway of Typhoon Maemi (2003). Typhoon Maemi tracked northwestward over Guam, turned North–Northeast towards the Korean peninsula on September 11, and it made landfall on the Korean peninsula on September 12. Subsequently, typhoon Maemi moved into the EJS and became extratropical and by September 15, the remnants were tracked over the Kamchatka Peninsula. The impact of the MYNN model on the TC-induced vertical mixing in the OBL was examined by comparing the results obtained by each turbulence model before and after Typhoon Maemi passed through the EJS.

A comparison of the observed and simulated SST before and after the typhoon had passed is shown in Figure 3. Before the typhoon passed over the EJS, the SST simulated using the two turbulence models showed a similar distribution to the observed data. However, there was a remarkable difference between the two parameterizations after the typhoon passed, particularly for the central part of the EJS and along the Japanese coast, indicated by a 22 °C isotherm. The SST simulated by the MY model was not sufficiently cooled by the typhoon compared to the observed data. Before the typhoon passed, the scatter diagram between the satellite-based SST data and the data simulated using the two vertical mixing parameterizations showed a good correlation, although the two mixing schemes typically yielded somewhat higher SSTs than the observed data (Figure 4a). However, after the typhoon passed, the difference between the observed and simulated SST in the MY model increased compared to the MYNN model (Figure 4b).

Figure 5 compares the vertical distribution of the daily mean temperature and zonal velocity along 133° E calculated using the two turbulence models before and after the typhoon passed. Before the typhoon event, the general distributions of the SST and zonal velocity in the two simulations were similar, although the MY model yielded a slightly shallower mixed layer and, consequently, a slightly warmer temperature in the upper ocean. However, a significant difference was visible after the typhoon event. The temperature obtained using the MYNN model was colder than that obtained using the MY model. The upper layer simulated by the MYNN model was well mixed vertically compared to the MY model, indicated by the southward movement of the 22.5 °C isotherm in the upper layer and a rising up the 10 °C isotherm at 100 m depth. A comparison of the mixed layer depth calculated using the two parameterizations showed that the mixed layer simulated by the MY model was not deeper after the impact. Alternatively, the MYNN model simulations showed a deepening along the typhoon track, indicating a response to the typhoon (Figure 6).

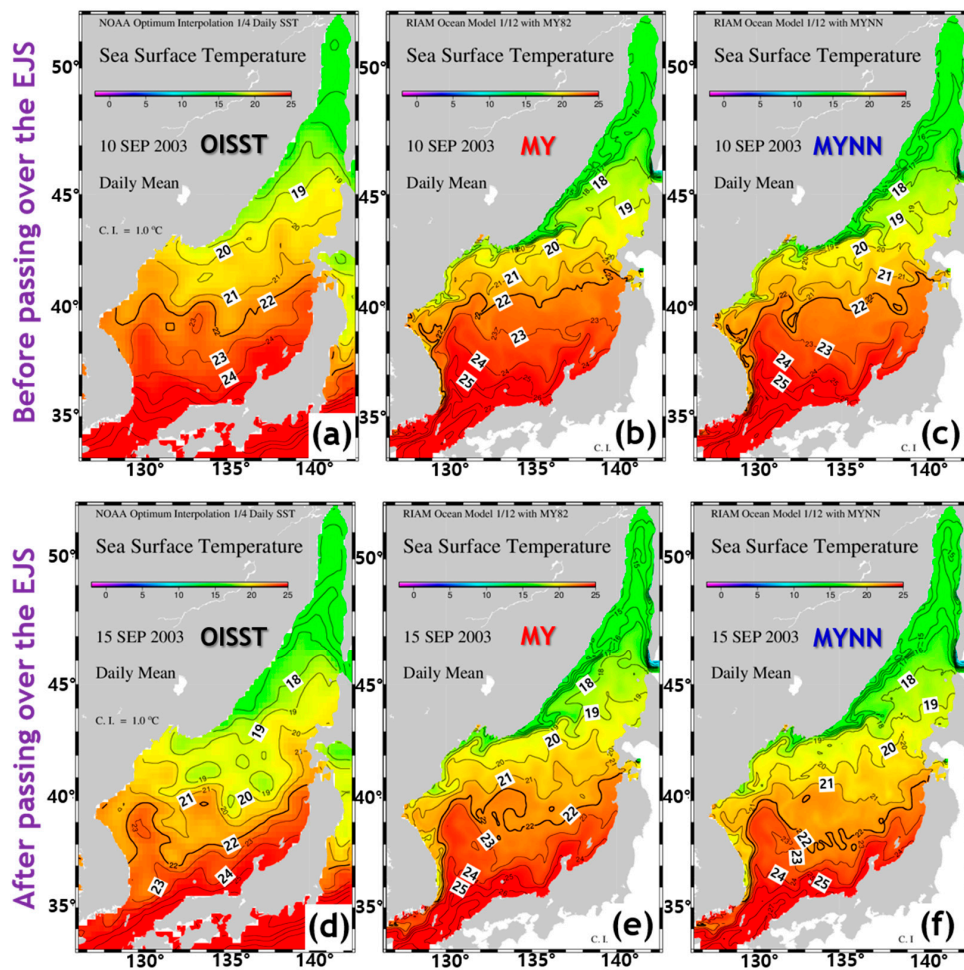


**Figure 3.** Sea surface temperature horizontal distributions obtained from (a,d) Optimum Interpolation Sea Surface Temperature (OISST) and simulated using (b,e) Mellor–Yamada (MY) model and (c,f) Mellor–Yamada–Nakanishi–Niino (MYNN) model before (top row) and after (bottom row) Typhoon Maemi. The thick contour line in each panel indicates a 22 °C isotherm. The contour interval is 1 °C.

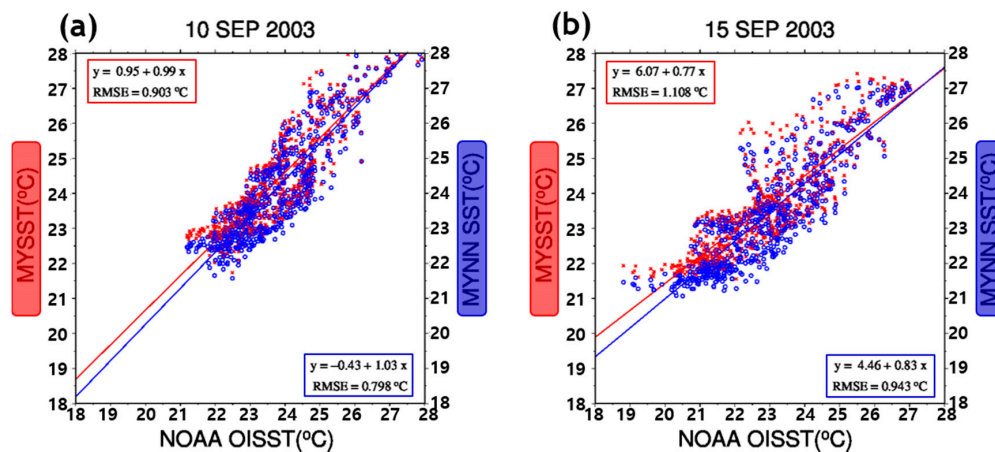


**Figure 4.** Scatter diagram between the sea surface temperatures (SSTs) south of 40° N obtained from satellite data and simulated using the Mellor–Yamada (MY) (red dots and line) and the Mellor–Yamada–Nakanishi–Niino (MYNN) (blue dots and line) models (a) before and (b) after Typhoon Maemi. (RMSE, root mean square error).

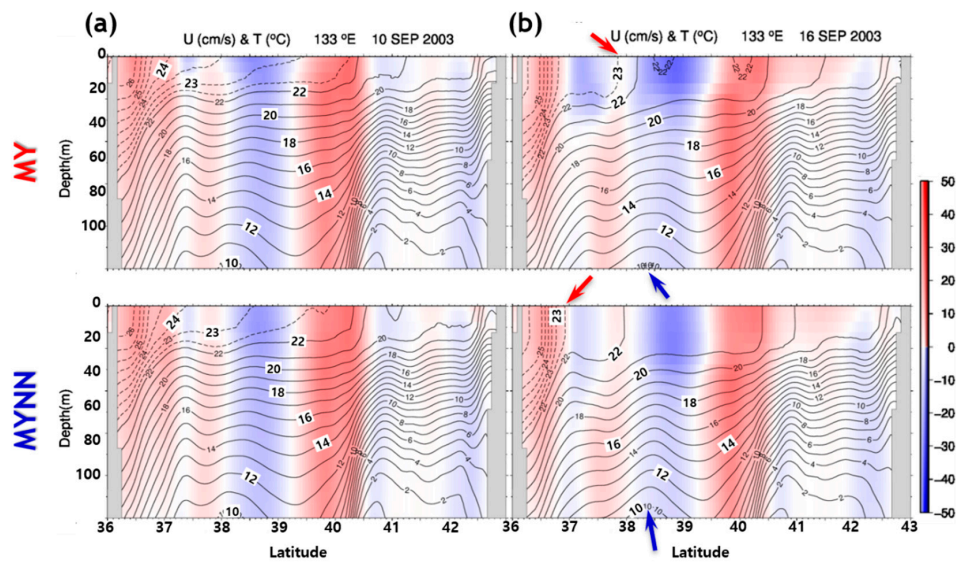


**Figure 5.** Vertical distribution of the temperature (contours) and zonal velocity (color-shaded) values calculated using the Mellor–Yamada (MY) (top row) and the Mellor–Yamada–Nakanishi–Niino (MYNN) (bottom row) models (a) before and (b) after Typhoon Maemi along the 133° E line (indicated by the solid blue line in Figure 1). The red arrow indicates the southward movement of the 22.5 °C isotherm in the upper layer and the blue arrow displays a rising of the 10 °C isotherm to a depth of 100 m. The solid contour line interval indicates 1 °C, and the dashed contour line interval indicates 0.5 °C.

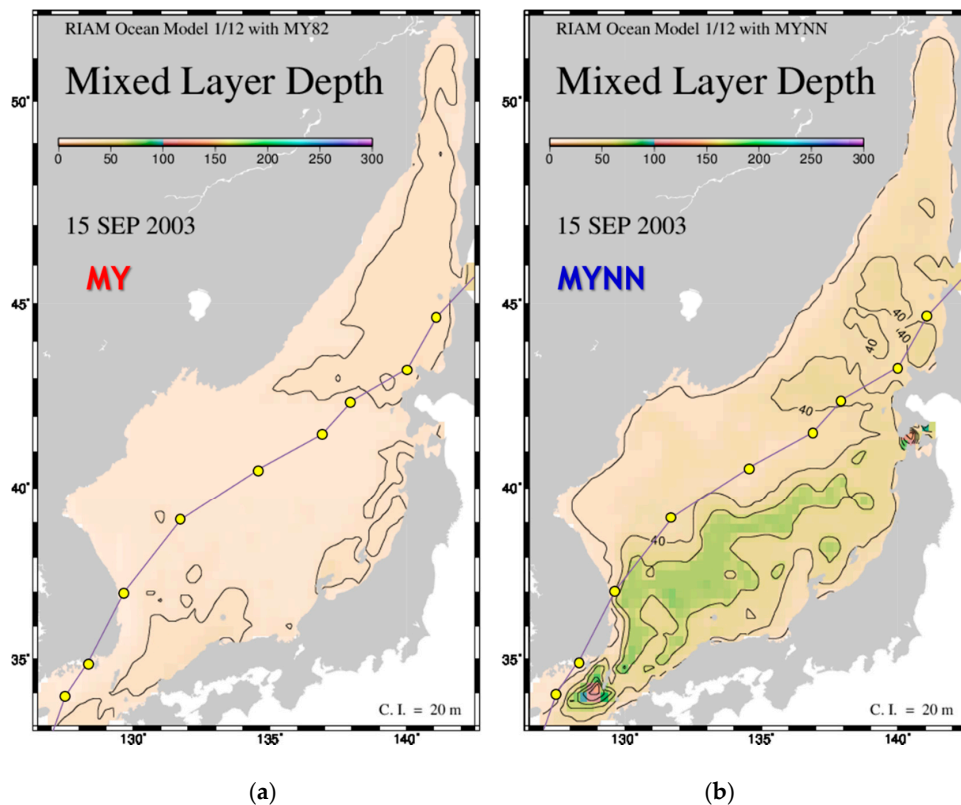


**Figure 6.** Horizontal distributions of the mixed layer depth calculated using (a) the Mellor–Yamada (MY) and (b) the Mellor–Yamada–Nakanishi–Niino (MYNN) models on September 15, 2003. The solid purple lines with yellow circles show the track of Typhoon Maemi. The contour interval is 20 m. The bottom of the surface mixed layer is defined at the depth where the potential temperature becomes lower than that at the sea surface by 0.5 °C.

#### 4.2. Enhancement of the Vertical Mixing

The temperature response in the upper layer to TCs is known to be largely the result of enhanced mixing associated with the near-inertial response to TC-related winds. TCs induce an energetic current with a strong inertial oscillation due to strong wind and wind vector rotation [51,52]. In addition, it is well known that there are significant near-inertial actions in the deep waters of the EJS [53]. Therefore, we need to better diagnose the vertical mixing induced by the near-inertial response in this region. Near-inertial internal waves triggered by TCs play an important role that drives turbulent mixing in the thermocline and ocean interior. A comparison of the near-inertial oscillations simulated by each turbulence model is shown in Figure 7. The figure shows the rotary spectra of the current velocity simulated by the MY and the MYNN model at depths of 29 and 1000 m at 133°40.7' E, 38°40.0' N (denoted by the red star in Figures 1 and 2). The rotary spectra calculated from both simulations showed that the near-inertial peak in the clockwise components is prominent at all depths, indicating that the peak frequency of the motion is slightly larger than the local inertial frequency,  $f$ . Interestingly, the super-inertial peak at around  $2f$  can be clearly observed in the result obtained using the MYNN model. These peaks at around  $2f$  have also been reported by Mori et al. [53], who found a general description of the near-inertial oscillations in the EJS by analyzing the observed current data. In addition, Niwa and Hibiya [54] reported that the double-inertial frequency waves emerged in the deep ocean interior at mid-latitudes. The existence of super-inertial waves is important because this super-inertial wave observed at around  $2f$  is believed to play a significant role in transferring energy to the internal wave field in the deep ocean and intensifies diapycnal mixing [54,55].

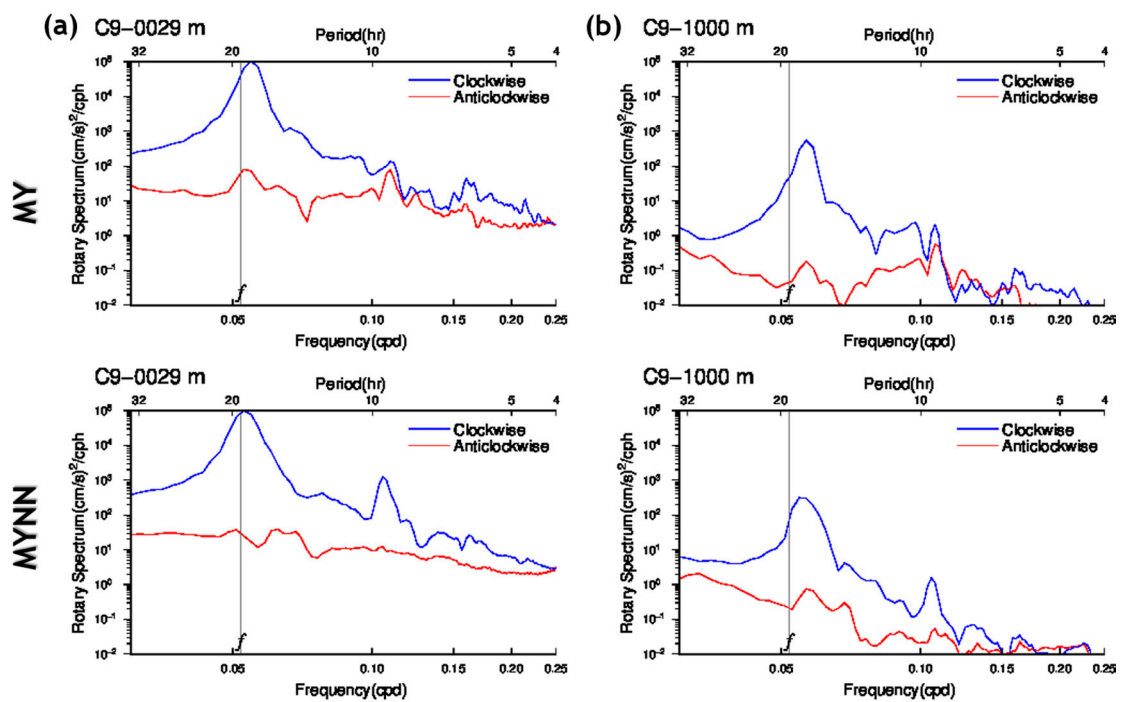


**Figure 7.** Rotary spectra of the current velocity simulated using the Mellor–Yamada (MY) (top row) and the Mellor–Yamada–Nakanishi–Niino (MYNN) (bottom row) models at depths of (a) 29 and (b) 1000 m at a point of 133°40.7' E, 38°40.0' N (denoted by the red star in Figures 1 and 2).

TC-induced winds generate intense kinetic energy in the upper ocean. The TC-generated kinetic energy is mostly consumed by vertical mixing between the surface warm water and the thermocline [56], but some of the kinetic energy input radiates into the ocean interior in the form of near-inertial internal waves [57]. The time evolutions of the band-pass filtered velocity and the near-inertial kinetic energy obtained using both simulations are shown in Figures 8 and 9, respectively. The cutoff of the band-pass

filter is  $\pm 1.75$  h from the inertial period at the site. The near-inertial component of the velocity at the surface layer obtained using the MY model was stronger than that obtained using the MYNN model. However, the MYNN simulated a stronger increase in the near-inertial currents at all depths except the surface. In the MYNN model, the depth of the mixed layer is thicker and the horizontal convergence in the layer increases with the depth of the mixed layer, and the lead-direct current becomes stronger. During both simulations, as the typhoon approaches, the near-inertial kinetic energy begins to increase in the upper layer from 8 September and then rises strongly after the typhoon impact from September 12. However, the pattern of increase in the near-inertial kinetic energy differs between the two simulations. The near-inertial kinetic energy simulated in the MYNN model increased dramatically at all depths when the typhoon reached the site (13 September).

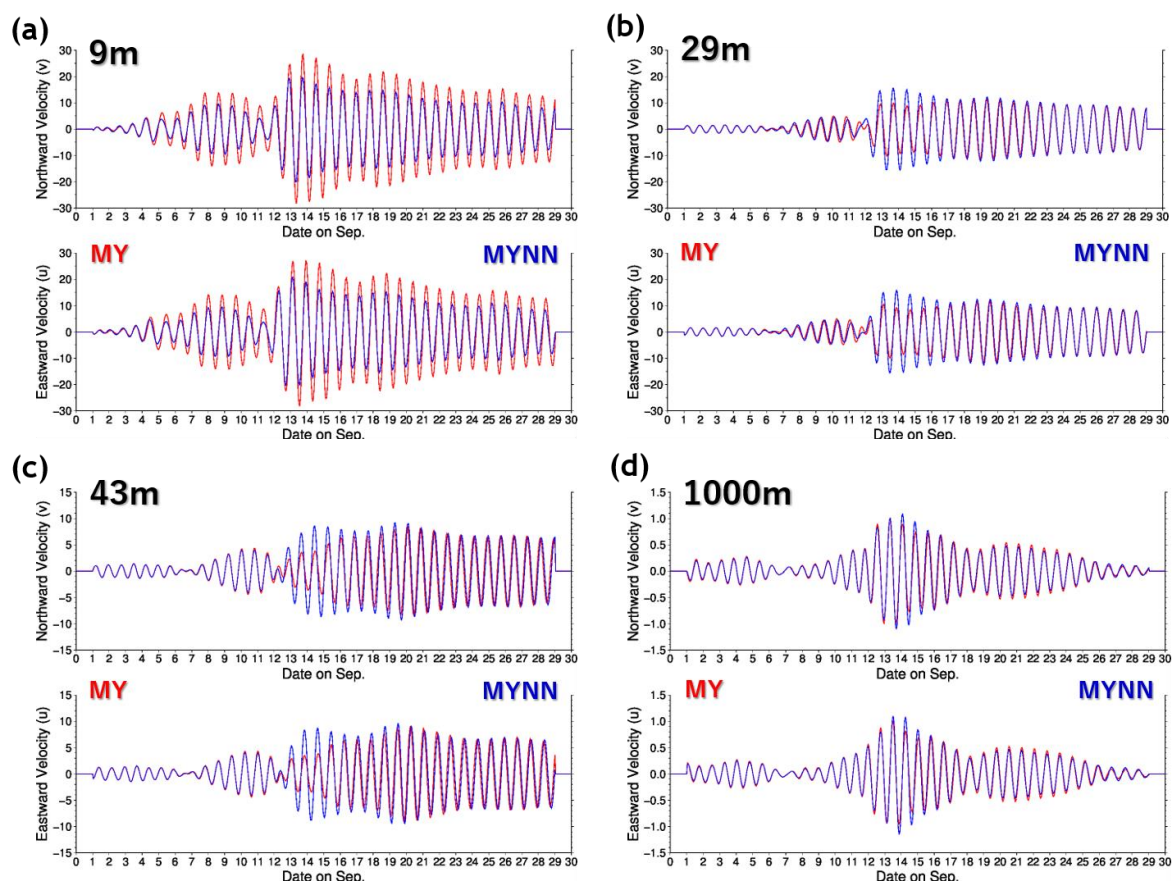


**Figure 8.** Time evolutions of the band-pass-filtered velocity simulated by the Mellor–Yamada (MY) (solid red line) and the Mellor–Yamada–Nakanishi–Niino (MYNN) (solid blue line) models at depths of (a) 9, (b) 29, (c) 43, and (d) 1000 m at a point of 133°40.7' E, 38°40.0' N (denoted by the red star in Figures 1 and 2). The top row in each panel is the meridional velocity, and the bottom row in each panel is the zonal velocity.

The near-inertial waves cause strong shear across the thermocline and produces mixing, which results in a deepening of the mixed layer and downward transport of heat. According to the results of this study, the MYNN model showed enhanced vertical propagation of the near-inertial activity from the mixed layer into the deeper ocean.

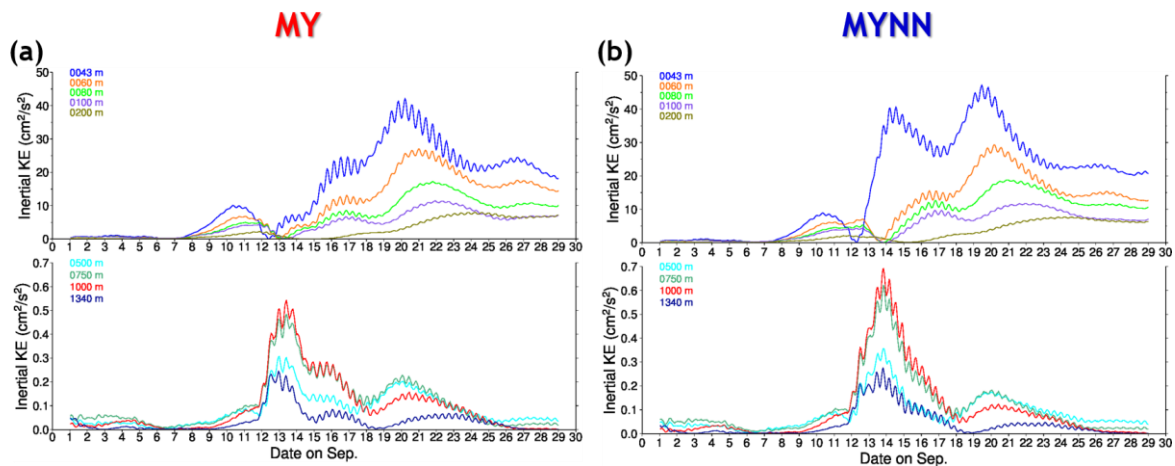


**Figure 9.** Time evolutions of the near-inertial kinetic energy simulated using (a) the Mellor–Yamada (MY) and (b) the Mellor–Yamada–Nakanishi–Niino (MYNN) models at several depths at a point of 133°40.7' E, 38°40.0' N. The top row in each panel is the upper layer (<200 m depth), and the bottom row in each panel is the lower layer (>500 m depth).

### 5. Summary and Discussion

Even though the MY model has been widely used in numerical experiments as well as operational numerical predictions, certain limitations in the model related to the atmospheric mixed layer have been identified by several studies. The two probable sources are the simplistic parameterization in the original MY closure formulation of the pressure correlations that appear in the equations for the second moments and the uncertain expression used for the length scale. The MYNN model has improved a number of limitations of the MY model by reflecting the buoyancy effects for the pressure covariances and by using a new diagnostic equation for  $l$ . It is worth noting that the closure constants and the diagnostic equation for TLS estimated by the MYNN are based on atmospheric LES results and they are employed for the OBL without any changes. However, previous studies with the MYNN, as mentioned in the Introduction, demonstrated that using original model parameters from the atmospheric MYNN also performs better than the MY in reproducing the vertical structure of the OBL. Nevertheless, it is necessary to reevaluate their applicability to the OBL.

In this study, we applied the improved MY model to an oceanic scenario and investigated the impact of the MYNN model for the oceanic mixed layer on TC-induced vertical mixing. To examine the improved MY model performance for the OBL, we incorporated the MY and MYNN models into the OGCM and performed two numerical experiments on the sensitivity of the OBL to the vertical mixing parameterization. Because TC-induced vertical mixing due to TC activity is responsible for significant alteration of the thermal conditions in the ocean, numerical simulations were constructed to compare the response of the OBL to each turbulence model caused by Typhoon Maemi (2003).

The SST simulated from the improved MY model agreed well with the observed data; such an agreement was not obtained from the original MY model. The MY model produced an extremely shallow mixed layer, and consequently, temperatures in the upper layer were excessively warm. This implies that the momentum and heat remaining at the surface layer can be transported downwards with the improved MY model. It is thought to be due to the revision of the  $L_S$  value to include the contributions of the stability at the surface layer, so that the  $L_S$  is larger above the unstable surface layer and smaller above the stable layer. Furthermore, a remarkable difference between the two models was found related to the inertial waves that are a substantial part of the ocean response to TCs. The rotary spectra calculated from both simulations showed that the near-inertial peak in the clockwise components was prominent at all depths. However, a super-inertial wave with a frequency of  $2f$ , playing a significant role in transferring energy to the internal wave field in the deep ocean and intensifying diapycnal mixing, is clearly seen in the MYNN model. In the MY model, the near-inertial component of the

velocity at the surface layer was stronger than that in the MYNN model. However, the MYNN simulated a stronger increase in the near-inertial currents at all depths except the surface. Furthermore, the near-inertial kinetic energy simulated in the MYNN increased dramatically at all depths when the typhoon arrived. Our results imply that the MYNN model can effectively produce the evolution of turbulence associated with the enhancement of TC-induced vertical mixing due to the new formulation of the TLS and the new expression for the stability functions, as well as the new closure constants.

In this study, we focus on TC-induced vertical mixing during a storm to investigate the impact of the improved MY model on oceanic vertical mixing because the largest changes in the OBL momentum budget and thermal conditions in the ocean are caused by strong synoptic scale storms. However, another issue in the MY model is mostly insufficient mixing during summer when wind is weak and stratification is strong [40,58]. Although not investigated in this study, to see how the MYNN model performs with the seasonal cycle is an interesting subject for future research.

**Author Contributions:** T.K. and J.-H.M. contributed equally to this work, including the conceptualization, theoretical methodology, the implementation of the software, the validation, writing the original draft, and the final supervision. All authors have read and agreed to the published version of the manuscript.

**Funding:** This research was supported by the Basic Science Research Program to Research Institute for Basic Science (RIBS) of Jeju National University through the National Research Foundation of Korea (NRF) funded by the Ministry of Education (2019R1A6A1A10072987) and is a part of the project titled “Improvement of management strategies on marine disturbing and harmful organisms (No. 20190518)”, funded by the Ministry of Oceans and Fisheries, Korea.

**Acknowledgments:** The authors express their gratitude to Jong-Hwan Yoon for his valuable comments and suggestions on this work and would like to thank editor and anonymous reviewers for their insightful comments and contributions to the manuscript.

**Conflicts of Interest:** The authors declare no conflict of interest.

## References

1. Kim, T.; Jin, E.K. Impact of an interactive ocean on numerical weather prediction: A case of a local heavy snowfall event in eastern Korea. *J. Geophys. Res. Atmos.* **2016**, *121*, 8243–8253. [[CrossRef](#)]
2. Kim, T.; Choo, S.-H.; Moon, J.-H.; Chang, P.-H. Contribution of tropical cyclones to abnormal sea surface temperature warming in the Yellow Sea in December 2004. *Dynam. Atmos. Ocean.* **2017**, *80*, 97–109. [[CrossRef](#)]
3. Kim, T.; Moon, J.-H.; Kang, K.R. Uncertainty and sensitivity of wave-induced sea surface roughness parameterisations for a coupled numerical weather prediction model. *Tellus A* **2018**, *70*, 1–18. [[CrossRef](#)]
4. Yamamoto, M.; Hirose, N. Possible modification of atmospheric circulation over the north-western Pacific induced by a small semi-enclosed ocean. *Geophys. Res. Lett.* **2011**, *38*, L03804. [[CrossRef](#)]
5. Kwon, Y.C.; Kim, T. Impact of air-sea exchange coefficients on the structure and intensity of tropical cyclones. *Terr. Atmos. Ocean. Sci.* **2017**, *28*, 345–356. [[CrossRef](#)]
6. Fisher, E.L. Hurricanes and the sea-surface temperature field. *J. Meteor.* **1958**, *15*, 328–333. [[CrossRef](#)]
7. Leipper, D.F. Observed ocean conditions and Hurricane Hilda, 1964. *J. Atmos. Sci.* **1967**, *24*, 182–196. [[CrossRef](#)]
8. D’Asaro, E.A. The energy flux from the wind to near-inertial motions in the surface mixed layer. *J. Phys. Oceanogr.* **1985**, *15*, 1043–1059. [[CrossRef](#)]
9. Kunze, E. The mean and near-inertial velocity fields in a warm-core ring. *J. Phys. Oceanogr.* **1986**, *16*, 1444–1461. [[CrossRef](#)]
10. D’Asaro, E.A. Upper-ocean inertial currents forced by a strong storm. Part III: Interaction of inertial currents and mesoscale eddies. *J. Phys. Oceanogr.* **1995**, *25*, 2953–2958. [[CrossRef](#)]
11. Lee, D.-K.; Niiler, P.P. The inertial chimney: The near-inertial energy drainage from the ocean surface to the deep layer. *J. Geophys. Res.* **1998**, *103*, 7579–7591. [[CrossRef](#)]
12. Garrett, C. What is the “near-inertial” band and why is it different from the rest of the internal wave spectrum? *J. Phys. Oceanogr.* **2001**, *31*, 962–971. [[CrossRef](#)]
13. Vincent, E.M.; Madec, G.; Lengaigne, M.; Vialard, J.; Koch-Larrouy, A. Influence of tropical cyclones on sea surface temperature seasonal cycle and ocean heat transport. *Clim. Dyn.* **2013**, *41*, 2019–2038. [[CrossRef](#)]

14. Mellor, G.L.; Yamada, T. A hierarchy of turbulence closure models for planetary boundary layers. *J. Atmos. Sci.* **1974**, *31*, 1791–1806. [[CrossRef](#)]
15. Mellor, G.L.; Yamada, T. Development of a turbulence closure model for geophysical fluid problems. *Rev. Geophys.* **1982**, *20*, 851–875. [[CrossRef](#)]
16. Mellor, G.L. One-dimensional ocean surface layer modeling a problem and a solution. *J. Phys. Oceanogr.* **2001**, *31*, 790–809. [[CrossRef](#)]
17. Mellor, G.L.; Blumberg, A.F. Wave breaking and ocean surface layer thermal response. *J. Phys. Oceanogr.* **2004**, *34*, 693–698. [[CrossRef](#)]
18. Mellor, G.L. Analytic prediction of the properties of stratified planetary surface layers. *J. Atmos. Sci.* **1973**, *30*, 1061–1069. [[CrossRef](#)]
19. Satoh, M.; Tomita, H.; Yashiro, H.; Miura, H.; Kodama, C.; Seiki, T.; Noda, A.T.; Yamada, Y.; Goto, D.; Sawada, M.; et al. The Non-hydrostatic Icosahedral Atmospheric Model: Description and development. *Prog. Earth Planet. Sci.* **2014**, *1*, 18. [[CrossRef](#)]
20. Nakano, M.; Wada, A.; Sawada, M.; Yoshimura, H.; Onishi, R.; Kawahara, S.; Sasaki, W.; Nasuno, T.; Yamaguchi, M.; Iriguchi, T.; et al. Global 7-km mesh nonhydrostatic Model Intercomparison Project for improving Typhoon forecast (TYMIP-G7): Experimental design and preliminary results. *Geosci. Model Dev.* **2017**, *10*, 1363–1381. [[CrossRef](#)]
21. Kukkonen, J.; Olsson, T.; Schultz, D.M.; Baklanov, A.; Klein, T.; Miranda, A.I.; Monteiro, A.; Hirtl, M.; Tarvainen, V.; Boy, M.; et al. A review of operational, regional-scale, chemical weather forecasting models in Europe. *Atmos. Chem. Phys.* **2012**, *12*, 1–87. [[CrossRef](#)]
22. Fox-Kemper, B.; Adcroft, A.; Böning, C.W.; Chassignet, E.P.; Curchitser, E.; Danabasoglu, G.; Eden, C.; England, M.H.; Gerdes, R.; Greatbatch, R.J.; et al. Challenges and Prospects in Ocean Circulation Models. *Front. Mar. Sci.* **2019**, *6*, 65. [[CrossRef](#)]
23. Sun, W.-Y.; Ogura, Y. Modeling the evolution of the convective planetary boundary layer. *J. Atmos. Sci.* **1980**, *37*, 1558–1572. [[CrossRef](#)]
24. Turton, J.; Brown, R. A comparison of a numerical model of radiation fog with detailed observations. *Q. J. R. Meteorol. Soc.* **1987**, *113*, 37–54. [[CrossRef](#)]
25. Galperin, B.; Kantha, L.H.; Rosati, A. A quasi-equilibrium turbulent energy model for geophysical flows. *J. Atmos. Sci.* **1988**, *45*, 55–62. [[CrossRef](#)]
26. Janjic, Z.I. The step-mountain coordinate: Physical package. *Mon. Weather Rev.* **1990**, *118*, 1429–1443. [[CrossRef](#)]
27. Janjic, Z.I. The step-mountain eta coordinate model: Further developments of the convection, viscous sublayer, and turbulence closure schemes. *Mon. Weather Rev.* **1994**, *122*, 927–945. [[CrossRef](#)]
28. Blumberg, A.F.; Galperin, B.G.; O'Connor, D.J. Modeling vertical structure of open channel flow. *J. Hydraul. Eng.* **1992**, *118*, 1119–1134. [[CrossRef](#)]
29. Kantha, L.H.; Clayson, C.A. An improved mixed layer model for geophysical applications. *J. Geophys. Res.* **1994**, *99*, 25235–25266. [[CrossRef](#)]
30. Nakanishi, M.; Niino, H. Development of an improved turbulence closure model for the atmospheric boundary layer. *J. Meteor. Soc. Jpn.* **2009**, *87*, 895–912. [[CrossRef](#)]
31. Nakanishi, M. Improvement of the Mellor-Yamada turbulence closure model based on large-eddy simulation data. *Bound.-Layer Meteor.* **2001**, *99*, 349–378. [[CrossRef](#)]
32. Hara, T. Update of the operational JMA mesoscale model and implementation of improved Mellor-Yamada level 3 scheme. In Proceedings of the Extended Abstracts, 22nd Conference on Weather Analysis and Forecasting/18th Conference on Numerical Weather Prediction, Park City, UT, USA, 25–29 June 2007; p. J3.5.
33. Saito, K.; Ishida, J.; Aranami, K.; Hara, T.; Segawa, T.; Narita, M.; Honda, Y. Nonhydrostatic atmospheric models and operational development at JMA. *J. Meteor. Soc. Jpn.* **2007**, *85*, 271–304. [[CrossRef](#)]
34. Chikira, M.; Mochizuki, T. Introduction of an improved Mellor-Yamada scheme into MIROC3.2. In Proceedings of the Preprints, Autumn Meeting of the Meteorological Society of Japan, Sapporo, Japan, 14–16 October 2007; p. 71. (In Japanese).
35. Furuichi, N.; Hibiya, T. Assessment of the upper-ocean mixed layer parameterizations using a large eddy simulation model. *J. Geophys. Res.* **2015**, *120*, 2350–2369. [[CrossRef](#)]
36. Furuichi, N.; Hibiya, T.; Niwa, Y. Assessment of turbulence closure models for resonant inertial response in the oceanic mixed layer using a large eddy simulation model. *J. Oceanogr.* **2012**, *68*, 285–294. [[CrossRef](#)]

37. Suzuki, S.; Niino, H.; Kimura, R. The mechanism of upper-oceanic vertical motions forced by a moving typhoon. *Fluid Dyn. Res.* **2011**, *43*, 025504. [[CrossRef](#)]
38. Shibano, R.; Yamanaka, Y.; Okada, N.; Chuda, T.; Suzuki, S.; Niino, H.; Toratani, M. Response of marine ecosystem to typhoon passage in the western subtropical North Pacific. *Geophys. Res. Lett.* **2011**, *38*, L18608. [[CrossRef](#)]
39. Kanada, S.; Tsujino, S.; Aiki, H.; Yoshioka, M.K.; Miyazawa, Y.; Tsuboki, K.; Takayabu, I. Impacts of SST Patterns on Rapid Intensification of Typhoon Megi (2010). *J. Geophys. Res. Atmos.* **2017**, *122*, 13245–13262. [[CrossRef](#)]
40. Ezer, T. On the seasonal mixed-layer simulated by a basin-scale ocean model and the Mellor-Yamada turbulence scheme. *J. Geophys. Res.* **2000**, *105*, 16843–16855. [[CrossRef](#)]
41. Huang, C.J.; Qiao, F.; Song, Z.; Ezer, T. Improving simulations of the upper ocean by inclusion of surface waves in Mellor-Yamada turbulence scheme. *J. Geophys. Res.* **2011**, *116*, C01007. [[CrossRef](#)]
42. Moeng, C.-H.; Wyngaard, J.C. Evaluation of turbulent transport and dissipation closures in second-order modelling. *J. Atmos. Sci.* **1989**, *46*, 2311–2330. [[CrossRef](#)]
43. Lee, H.C. A Numerical Simulation for the Water Masses and Circulations of the Yellow Sea and the East China Sea. Ph.D. Thesis, Kyushu University, Fukuoka, Japan, 1996.
44. Choi, B.H.; Kim, K.O.; Eum, H.M. Digital bathymetric and topographic data for neighboring seas of Korea. *J. Korean Soc. Coastal Ocean Eng.* **2002**, *14*, 41–50. (In Korean)
45. Kim, T.; Yoon, J.-H. Seasonal variation of upper layer circulation in the northern part of the East/Japan Sea. *Cont. Shelf Res.* **2010**, *30*, 1283–1301. [[CrossRef](#)]
46. Typhoon Research Center Home Page. Available online: <http://www.typhoon.or.kr/> (accessed on 17 May 2020).
47. Saito, K.; Fujita, T.; Yamada, Y.; Ishida, J.; Kumagai, Y.; Aranami, K.; Ohmori, S.; Nagasawa, R.; Kumagai, S.; Muroi, C.; et al. The operational JMA nonhydrostatic mesoscale model. *Mon. Weather Rev.* **2006**, *134*, 1266–1298. [[CrossRef](#)]
48. Hirose, N.; Takayama, K.; Moon, J.-H.; Watanabe, T.; Nishida, Y. Regional data assimilation system extended to the East Asian marginal seas. *Umi Sora (Sea and Sky)* **2013**, *89*, 43–51.
49. Takikawa, T.; Yoon, J.-H.; Cho, K.-D. The Tsushima Warm Current through Tsushima Straits estimated from ferryboat. *J. Phys. Oceanogr.* **2005**, *35*, 1154–1168. [[CrossRef](#)]
50. Hirose, N.; Kawamura, H.; Lee, H.J.; Yoon, J.-H. Sequential forecasting of the surface and subsurface conditions in the Japan Sea. *J. Oceanogr.* **2007**, *63*, 467–481. [[CrossRef](#)]
51. Price, J.F. Upper ocean response to a hurricane. *J. Phy. Oceanogr.* **1981**, *11*, 153–175. [[CrossRef](#)]
52. Price, J.F. Internal wave wake of a moving storm. Part I: Scales, energy budget and observations. *J. Phys. Oceanogr.* **1983**, *13*, 949–965. [[CrossRef](#)]
53. Mori, K.; Matsuno, T.; Senjyu, T. Seasonal/Spatial Variations of the Near-Inertial Oscillations in the Deep Water of the Japan Sea. *J. Oceanogr.* **2005**, *61*, 761–773. [[CrossRef](#)]
54. Niwa, Y.; Hibiya, T. Nonlinear processes of energy transfer from traveling hurricanes to the deep ocean internal wave field. *J. Geophys. Res.* **1997**, *102*, 12469–12477. [[CrossRef](#)]
55. Danioux, E.; Klein, P.; Rivière, P. Propagation of wind energy into the deep ocean through a fully turbulent mesoscale eddy field. *J. Phys. Oceanogr.* **2008**, *38*, 2224–2241. [[CrossRef](#)]
56. Jaimes, B.; Shay, L.K. Mixed layer cooling in mesoscale oceanic eddies during Hurricanes Katrina and Rita. *Mon. Weather Rev.* **2009**, *137*, 4188–4207. [[CrossRef](#)]
57. Cuypers, Y.; Le Vaillant, X.; Bouruet-Aubertot, P.; Vialard, J.; McPhaden, M. Tropical storm-induced near inertial internal waves during the Cirene experiment: Energy fluxes and impact on vertical mixing. *J. Geophys. Res.* **2013**, *118*, 358–380. [[CrossRef](#)]
58. Martin, P.J. Simulation of the mixed layer at OWS November and Papa with several models. *J. Geoph. Res.* **1985**, *90*, 903–916. [[CrossRef](#)]

